© 2020. Published by The Company of Biologists Ltd | Development (2020) 147, dev190512. doi:10.1242/dev.190512

STEM CELLS AND REGENERATION

RESEARCH ARTICLE

Connexin 43 gap junctional intercellular communication inhibits *evx1* expression and joint formation in regenerating fins

Shashwati Bhattacharya*, Caitlin Hyland, Matthias M. Falk and M. Kathryn Iovine*

ABSTRACT

The gap junction protein Connexin 43 (Cx43) contributes to cell fate decisions that determine the location of fin ray joints during regeneration. Here, we provide insights into how Cx43, expressed medially, influences changes in gene expression in lateral skeletal precursor cells. Using the Gap27 peptide inhibitor specific to Cx43, we show that Cx43-gap junctional intercellular communication (GJIC) influences Cx43-dependent skeletal phenotypes, including segment length. We also demonstrate that Cx43-GJIC influences the expression of the Smp/β-catenin pathway in the lateral skeletal precursor cells, and does not influence the Sema3d pathway. Moreover, we show that the *cx43*^{lh10} allele, which has increased Cx43 protein levels, exhibits increased regenerate length and segment length. These phenotypes are rescued by Gap27, suggesting that increased Cx43 is responsible for the observed Cx43 phenotypes. Finally, our findings suggest that inhibition of Cx43 hemichannel activity does not influence Cx43-dependent skeletal phenotypes. These data provide evidence that Cx43-GJIC is responsible for regulating cell fate decisions associated with appropriate joint formation in the regenerating fin.

KEY WORDS: GJIC, Connexin 43, Skeletal regeneration, Zebrafish

INTRODUCTION

Skeletal patterning requires both the formation of correctly sized and shaped bones, and the appropriate positioning of the joints. The correct placement of joints is crucial to provide the skeleton with flexibility. Molecular mechanisms determining the location of synovial joints are poorly understood (Rux et al., 2019). The first indication that a joint will form is the condensation of a discrete band of chondrocytes called the 'interzone'. However, the signals responsible for initiating differentiation in cells that establish the interzone remain elusive. We use the zebrafish regenerating fin to address the fundamental issue of how joints develop at the appropriate location. The zebrafish caudal fin is composed of multiple bony fin rays; each bony ray is made up of bony segments flanked by joints. The fin is therefore a rich source of joints. Furthermore, regeneration proceeds rapidly following amputation (reviewed by Wehner and Weidinger, 2015). Wound healing occurs within 24 h post-amputation (hpa), followed by the establishment of the blastema (i.e. rapidly dividing cells). Outgrowth and differentiation proceed until regeneration is complete (~2 weeks). The blastema is located distally in the medial mesenchyme, whereas skeletal differentiation occurs in the lateral mesenchyme. Both osteoblasts and joint-forming cells are derived from a common skeletal precursor cell (SPC) (Tu and Johnson, 2011). SPCs that will become joint-forming cells express *even-skipped homeobox 1* (*evx1*), which is required for joint formation (Borday et al., 2001; Schulte et al., 2011). Manipulation of *evx1* influences segment length in a predictable manner. Less *evx1* leads to delayed joint formation and longer segments; more *evx1* leads to premature joint formation and shorter segments (Dardis et al., 2017). Therefore, *evx1* expression is a reliable indicator of the joint-forming cell fate.

Previous research on two fin length mutants, *short fin*^{b123} (*sof*^{b123}) and *another long fin*^{dty86} (*alf*^{dty86}), indicates that Cx43 contributes to determining joint location. The *sof*^{b123} mutant has a hypomorphic mutation in the *cx43* gene that causes reduced fin length, reduced segment length and reduced cell proliferation (Hoptak-Solga et al., 2008; Iovine et al., 2005). The *alf*^{dty86} mutant exhibits increased *cx43* expression and shows stochastic joint failure (i.e. longer segment length on average, Sims et al., 2009). The *alf*^{dty86} mutation is in the *kcnk5b* gene (Perathoner et al., 2014). However, because knockdown of Cx43 in *alf*^{dty86} rescues the joint failure phenotype (Sims et al., 2009), joint failure appears to be the result of increased *cx43* expression. Together, these studies indicate that Cx43 suppresses joint formation, and that the short segment phenotype of *sof*^{b123} is the result of premature joint formation. We have suggested that the gap junction protein Connexin 43 (Cx43) influences the specification of cell fate in SPCs by regulating the expression of *evx1* (Dardis et al., 2017; Bhattacharya et al., 2018). Thus, high Cx43 favors the differentiation of SPCs into osteoblasts (and *evx1* is reduced), whereas lower Cx43 favors the differentiation of SPCs into joint-forming cells (and *evx1* is increased) (Dardis et al., 2017).

In order to provide insights into how Cx43 influences *evx1* expression and joint formation, we previously identified changes in gene expression downstream of *cx43*. For example, we found that the *semaphorin3d* (*sema3d*) gene is molecularly and functionally downstream of *cx43* (Ton and Iovine, 2012). Sema3d is a secreted growth factor; in our previous study we suggested that Sema3d interacts with the plexin A3 receptor to influence *evx1* expression in SPCs. More recently, we showed that *simplet* (*smp*) is molecularly and functionally downstream of *cx43* (Bhattacharya et al., 2018). Smp protein brings β-catenin into the nucleus to regulate gene expression (Kizil et al., 2014). Indeed, β-catenin signaling is also downstream of *cx43* and contributes to determining segment length (Bhattacharya et al., 2018). Although *cx43* acts upstream of both *sema3d* and *smp*, it is notable that these genes are not expressed in the same cellular compartments. Both *cx43* mRNA and Cx43 protein are expressed mainly in the medial mesenchyme but also in a discrete group of lateral cells (Sims et al., 2009; Ton and Iovine, 2013), whereas *sema3d* is expressed in the lateral SPCs (Ton and Iovine, 2012). The *smp* mRNA is expressed in the lateral SPCs but also in the distal blastema, the wound epidermis and basal layer of

Department of Biological Sciences, Lehigh University, Bethlehem, PA 18020, USA.

*Authors for correspondence (mki3@lehigh.edu; shb215@lehigh.edu)

M.K.I., 0000-0003-0046-8482

Handling Editor: Liz Robertson
Received 12 March 2020; Accepted 5 June 2020

Development (2020) 147, dev190512. doi:10.1242/dev.190512

the epidermis. However, β-catenin signaling is limited to the lateral mesenchyme and distalmost medial mesenchyme (Stewart et al., 2014; Wehner et al., 2014). Consequently, the role of Smp during joint location is probably limited to the lateral mesenchyme. Together, our previous findings support a model in which Cx43 influences changes in gene expression in SPCs (i.e. *smp* and/or *sema3d*) that, in turn, lead to the suppression of *evx1* (i.e. perhaps via β-catenin-mediated transcriptional regulation). It is of interest to discover whether the proposed Sema3d signaling pathway regulates the expression of *smp* in SPCs.

We demonstrated that medially expressed Cx43 influences joint formation using clonal analyses. Cells expressing wild-type Cx43 were introduced into *sof*^{b123} embryos, and skeletal phenotypes were evaluated in adult regenerating fins. Remarkably, only medially expressed Cx43 could rescue the *sof*^{b123} regenerate length and segment length phenotypes (Dardis et al., 2017). Thus, medial Cx43 appears to influence cell fate decisions in the lateral compartment. Gap junctions have several functions, including gap junctional intercellular communication (GJIC), hemichannel activity and serving as a scaffold for signal transduction proteins (Goodenough et al., 1996; Jiang and Gu, 2005; Moorer et al., 2017; Sáez et al., 2005). Here, we show that Cx43-GJIC influences skeletal regenerate length and segment length phenotypes, as well as changes in gene expression. This was tested using both inhibition of Cx43-GJIC and overactivation of Cx43-GJIC. We also show that Cx43 hemichannel activity is not sufficient to influence skeletal phenotypes during fin regeneration. Overall, these findings provide significant new insights into how Cx43 influences changes in gene expression required for SPC cell fate decisions and joint formation.

RESULTS

Cx43-GJIC regulates fin regeneration and joint formation

To test the possibility that Cx43-GJIC in the medial mesenchyme influences skeletal phenotypes, we inhibited Cx43-GJIC using the peptide-inhibitor Gap27. Gap27 binds the second extracellular loop of Cx43 and specifically inhibits the formation of gap junctions and GJIC (Warner et al., 1995) (Fig. 1A). Notably, the sequence targeted by Gap27 is identical between human and zebrafish Cx43. We first injected a labeled version of Gap27 (i.e. 5Fam-Gap27) to confirm the extracellular localization of Gap27 in the mesenchymal compartment of the fin rays. Wild-type regenerating fins at 72 hpa were injected with 5Fam-Gap27 and harvested 24 h after injection. Fins were fixed and processed for cryosectioning. We observed that 5Fam-Gap27 was broadly distributed, including in the mesenchyme and at the cell periphery (Fig. 1B). Although Gap27 is found outside the medial mesenchyme, our previous clonal analyses reveal that only Cx43 function in the medial cells contributes to segment length and regenerate length (Dardis et al., 2017).

Next, to test the effect of Cx43-GJIC inhibition, we injected either unlabeled Gap27 or 5Fam-Gap27 into half of the fin rays of wild-type regenerating fins at 72 hpa, leaving the other half as an internal control. Alternatively, we similarly injected a scrambled Gap27 (Scrm-Gap27) peptide as a negative control. Regenerate length and segment length were evaluated at 7 days post-amputation (dpa) by measuring only from the third fin ray in each lobe, which we established as standard practice (Iovine and Johnson, 2000). To minimize fin to fin variation, we used the percentage similarity method to determine whether the peptide had an effect (i.e. Bhattacharya et al., 2018; Govindan et al., 2016). We measured the ratio of the injected side to the uninjected side reported as a percentage. Values close to 100% indicated little effect of the peptide, whereas values significantly different from 100% revealed that the peptide influences skeletal phenotypes. Importantly, we observed a significant reduction in both regenerate length and segment length in Gap27-injected fins (i.e. unlabeled-Gap27 or 5-Fam-Gap27) compared with the Scrm-Gap27 injection (Fig. 1C,D,F,G). These data indicate that the 5-Fam tag does not impair the function of the Gap27 peptide, and that the Gap27 peptide is sufficient to inhibit regenerate length and segment length. We used unlabeled Gap27 for further studies.

The effect of Gap27 on cell proliferation was evaluated by monitoring histone-3-phosphate (H3P) staining, which is a marker for mitotic cells (Wei et al., 1999). Either Gap27 or Scrm-Gap27 was injected as described above, followed by processing for H3P immunofluorescence. In addition, using the percent similarity method, we found that cell proliferation was significantly reduced in Gap27-injected fins compared with the Scrm-Gap27-injected fins (Fig. 1E,H). Thus, Gap27 injection recapitulates the phenotypes of *sof*^{b123} (Hoptak-Solga et al., 2008; Iovine et al., 2005). We conclude that Cx43-GJIC contributes to the Cx43-dependent skeletal phenotypes of regenerate length, segment length and cell proliferation.

Cx43-GJIC influences Smp/β-catenin signaling

Previously, we identified both Smp and Sema3d pathways acting downstream of Cx43 during joint formation (Bhattacharya et al., 2018; Ton and Iovine, 2012). To address whether Smp and Sema3d function in a common pathway downstream of Cx43, we tested for evidence of synergy by co-injecting subthreshold doses of both gene-targeting morpholinos (MOs). We identified 0.5 mM Smp-MO as the subthreshold dose (Bhattacharya et al., 2018) and 0.25 mM Sema3d-MO as the subthreshold dose (Govindan et al., 2016). We co-injected subthreshold doses of Sema3d-MO and Smp-MO in 72 hpa regenerating fins and measured segment length and regenerate length at 7 dpa. Because the double-injected fins did not exhibit more severe phenotypes than either set of single-injected fins, we conclude that there is no evidence of synergy between Sema3d and Smp. This indicates that Sema3d and Smp act in independent pathways downstream of Cx43 (Fig. S1). After finding that *sema3d* and *smp* are regulated by independent Cx43-mediated pathways, we decided to investigate whether either or both of these pathways are regulated by Cx43-GJIC (Fig. 2A). We therefore tested for synergy between Gap27 and Smp, and between Gap27 and Sema3d. We identified 0.25 mM as the subthreshold dose of Gap27. Co-injection of Gap27 and Smp-MO subthreshold doses revealed significantly reduced segment length and regenerate length when compared with single injections of either Smp-MO or Gap27 alone (Fig. 2B). These findings provide evidence for synergy between Cx43-GJIC and Smp, supporting the conclusion that Smp and Cx43-GJIC function together in a common molecular pathway to regulate Cx43-dependent phenotypes. In contrast, we did not find evidence of synergy between Cx43-GJIC and Sema3d (Fig. 2C). Together, these findings indicate that Cx43-GJIC influences the Smp/β-catenin pathway, and not the Sema3d pathway, during joint formation.

To confirm this finding, we next evaluated changes in gene expression downstream of Cx43-GJIC. If Cx43-GJIC influences joint formation via Smp/β-catenin, we expect that inhibiting Cx43-GJIC will lead to reduced *smp* and increased *evx1* expression (Fig. 3A). We evaluated *smp* and *evx1* expression by whole-mount *in-situ* hybridization in Gap27- and Scrm-Gap27-injected fins. As predicted, we found that *smp* expression is reduced in Gap27-injected fins compared with Scrm-Gap27-injected fins (Fig. 3B). To evaluate *evx1* expression, we calculated the frequency of *evx1*-positive fin rays across regenerating fins (Dardis et al., 2017; Ton

Development (2020) 147, dev190512. doi:10.1242/dev.190512

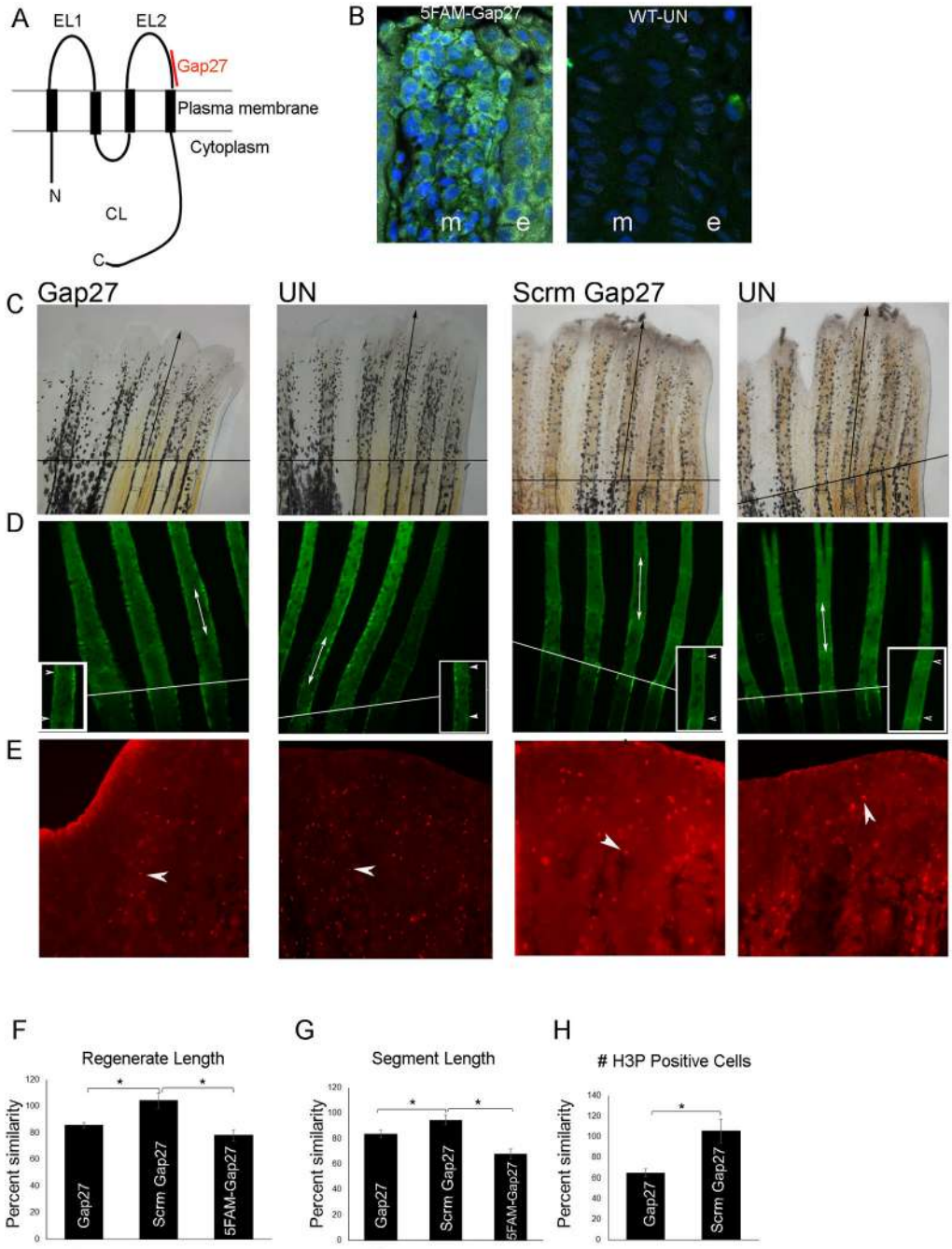

Fig. 1. Inhibition of Cx43-GJIC recapitulates *sof*^{b123} phenotypes. (A) Schematic of Cx43 showing the location of Gap27 interaction with the second extracellular loop. N, amino terminus; C, carboxy terminus; EL1/EL2, extracellular loop1/2; CL, cytoplasmic loop. (B) Representative longitudinal cross-sections showing localization of 5FAM-Gap27 (green) following its injection. DAPI (blue) stains cell nuclei. m, mesenchyme; e, epidermis. UN, uninjected. (C) Regenerate length is reduced in Gap27-injected fins compared with Scrm-Gap27-injected fins. All fins were amputated at the 50% level. The amputation plane is indicated (black line). Black arrow indicates the distance from the amputation plane to the distal tip of the third fin ray. Injections were performed at 3 dpa and measurements were taken at 7 dpa. UN, uninjected. Bar graph (F) shows a significant reduction in the percentage similarity between Gap27 and Scrm-Gap27 (one-way ANOVA with Tukey's and Dunnett's multiple comparison as post-hoc tests; **P*<0.05). *n*=21; three independent replicates. (D) Calcein-stained fin rays show reduced segment length in Gap27-injected fins compared with Scrm-Gap27-injected fins. Arrows and arrowheads point to the first two joints following the amputation plane (white line). The inset shows a higher magnification of the segments. Bar graph (G) reveals a significant reduction in the percentage similarity between Gap27 and Scrm-Gap27 (one-way ANOVA with Tukey's and Dunnett's multiple comparison as post-hoc tests; **P*<0.05). *n*=19; three independent replicates. (E) H3P^{+} cells are reduced in number in Gap27-injected fins compared with Scrm-Gap27-injected fins. Arrowheads identify one H3P^{+} cell per image. Bar graph (H) reveals a significant reduction in the percentage similarity between Gap27 and Scrm-Gap27. Student's *t*-test, two tailed and unpaired, **P*<0.05 (*n*=23, three independent replicates). Data are mean±s.e.m.

and Iovine, 2013). An increase in the percentage of *evx1*-positive fin rays reflects an increase in *evx1* expression. Indeed, the percentage of *evx1*-positive fin rays increased in the Gap27-injected fins compared with the Scrm-Gap27-injected fins (Fig. 3C,D). Thus, the inhibition of Cx43-GJIC reduces *smp* expression and increases *evx1* expression, mimicking *sof*^{b123}.

Development (2020) 147, dev190512. doi:10.1242/dev.190512

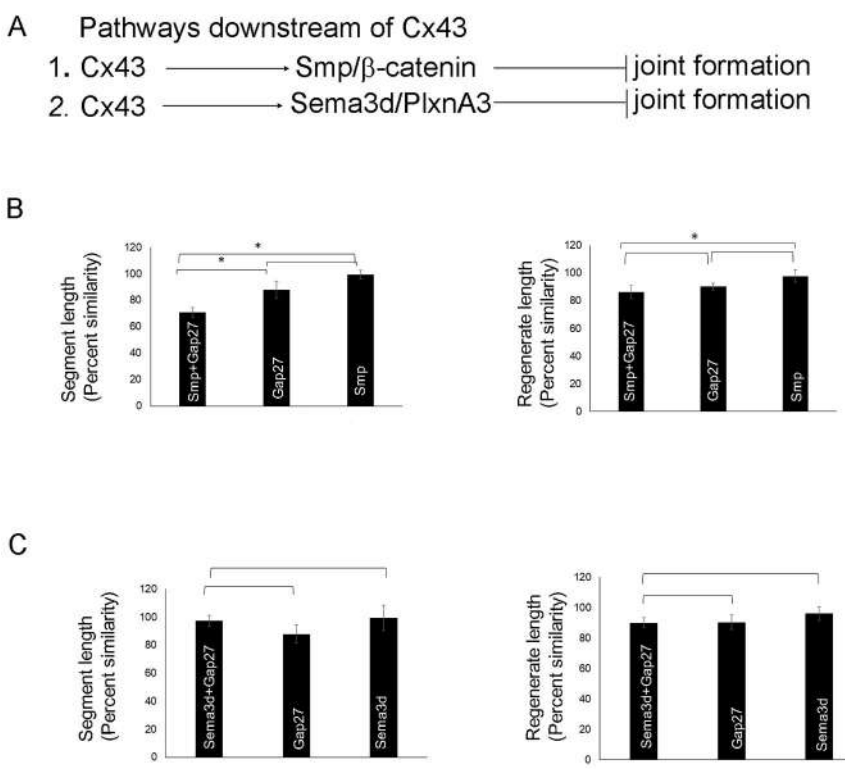

Fig. 2. Cx43-GJIC and Smp act in a common pathway. (A) Two previously described Cx43-dependent pathways impinging on joint formation. (B) Smp-KD and Gap27 exhibit synergistic effects on both segment length and regenerate length. Treatment with subthreshold doses of both Smp-MO and Gap27 lead to reduced segment length and regenerate length compared with either single treatment (one-way ANOVA with Tukey's multiple comparison as post-hoc test; **P*<0.05). *n*=16; three independent replicates. (C) Sema3d-KD and Gap27 fail to exhibit synergistic effects for either segment length or regenerate length. Treatment with subthreshold doses of both Sema3d-MO and Gap27 are not significantly different from either single treatment (one-way ANOVA with Tukey's multiple comparison as post-hoc test; **P*<0.05) (*n*=16, three independent replicates). Data are mean±s.e.m.

Because *smp* levels were reduced in Gap27-injected fins, we further expected active β-catenin levels to be reduced in Gap27-injected fins. We prepared total fin lysates from Gap27- and Scrm-Gap27-injected fins, and evaluated active (i.e. non-phosphorylated) β-catenin levels by immunoblotting. We found that the amount of active β-catenin is decreased in Gap27-injected lysates by 39% compared with Scrm-Gap27-injected lysates (Fig. 4).

Increased Cx43-GJIC suppresses joint formation and leads to long segments

To test whether increasing Cx43-GJIC influences joint formation, we used the recently established *cx43*^{lh10} allele, which contains a deletion of amino acids 256-289 from the Cx43 carboxy tail. A similar deletion in human Cx43 inhibits Cx43 turnover, doubling its half-life when expressed in HeLa cells (i.e. Cx43-Δ254-290,

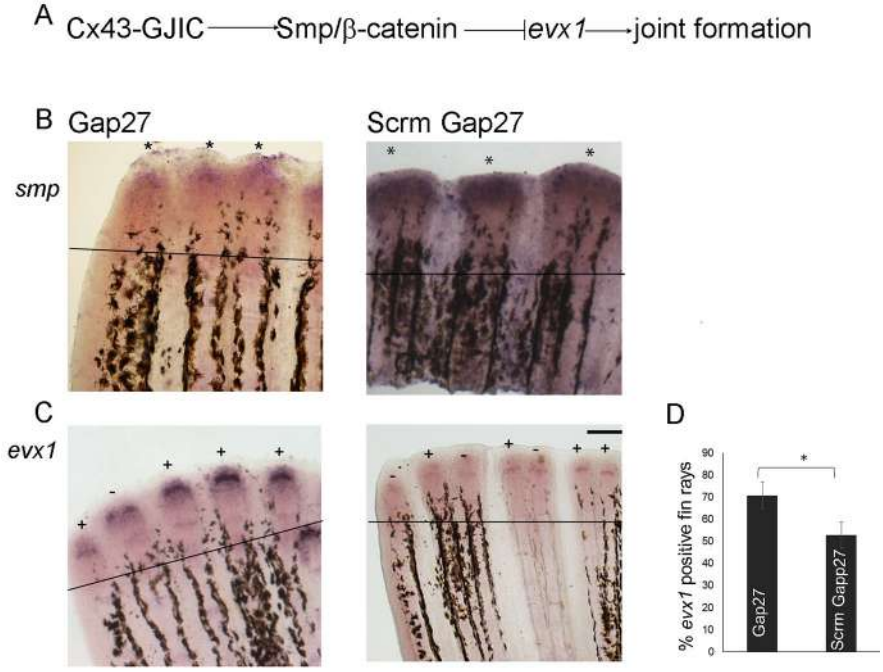

Fig. 3. Cx43-GJIC influences changes in gene expression. (A) Proposed pathway for changes in gene expression influenced by Cx43-GJIC. (B) Gap27 injections lead to reduced *smp* expression compared with Scrm-Gap27 injections (*n*=15). Asterisks indicate identification of stained fin rays. (C) Gap27 injections lead to increased frequency of *evx1* expression compared with Scrm-Gap27 injections (*n*=10, three independent replicates). + indicates fin rays positive for *evx1*; – indicates fin rays negative for *evx1*. (D) Bar graph showing increased percentage of *evx1*$^{+}$ fin rays with Gap27 injections compared with Scrm-Gap27 injections (Student's *t*-test, two tailed and unpaired, **P*<0.05). *n*=16; three independent replicates. Data are mean±s.e.m. Scale bar: 50 µm.

Development (2020) 147, dev190512. doi:10.1242/dev.190512

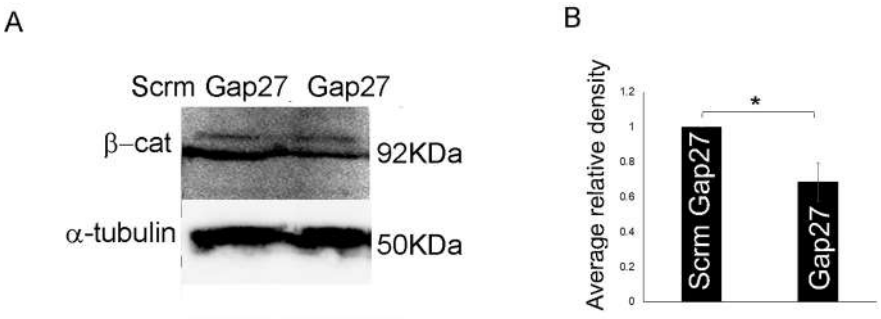

Fig. 4. Cx43-GJIC influences active β-catenin levels. (A) Immunoblots showing reduced active β-catenin in Gap27-injected fins compared with Scrm-Gap27-injected fins. (B) Bar graph showing the average relative densities of the β-catenin bands between experimental and control samples from three biological replicates. The amount of active β-catenin is reduced by 39% in Gap27-injected lysates (Student's *t*-test, two tailed and unpaired, **P*<0.05). Ten fins per lysate; three independent replicates. Data are mean± s.e.m.

Fong et al., 2013). We generated the zebrafish deletion allele using CRISPR/Cas9, and the in-frame deletion was validated by sequencing. We first confirmed that Cx43 protein levels were increased in the *cx43*^{lh10} line by preparing fin lysates and monitoring total Cx43 protein levels. We found a ∼45% increase in Cx43 protein in *cx43*^{lh10} compared with wild-type regenerating fins (Fig. 5). We next evaluated skeletal phenotypes in the *cx43*^{lh10} allele (Fig. 6A) by amputating fins at 50% and measuring regenerate length and segment length at 7 dpa. Regenerating fins in the *cx43*^{lh10} line exhibited a significant increase in both regenerate length and segment length compared with wild-type fins (Fig. 6B,C). Next, we monitored *evx1* expression to establish that the observed increase in segment length functions through our previously defined pathway. We measured levels of *evx1* via *in situ* hybridization and found that *cx43*^{lh10} fins express *evx1* expression in fewer fin rays compared with wild-type fins, consistent with increased Cx43-GJIC (Fig. 6D).

To determine whether increased Cx43-GJIC was in fact responsible for the increased segment length phenotype in the *cx43*^{lh10} line, we tested whether Gap27 injections could abrogate this phenotype. We injected Gap27 peptide into half of the fin rays in the *cx43*^{lh10} line at 72 hpa, leaving the other half as an internal control. Alternatively, the Scrm-Gap27 peptide was similarly injected as a negative control. We observed a significant reduction in regenerate length and segment length in Gap27-injected fins compared with the Scrm-Gap27 injected fins (Fig. 7A,B). Therefore, Cx43-GJIC appears to be responsible for the long segment phenotype in the *cx43*^{lh10} line.

Cx43 hemichannel activity does not influence skeletal growth and patterning

To test the role of Cx43-hemichannel activity in fin regeneration and joint positioning, we used the peptide Gap19, which binds to the Cx43-intracellular loop and inhibits hemichannel activity (Wang et al., 2013). The targeted sequence in zebrafish Cx43 differs slightly from human Cx43 (KK**I**ELK**K**FK in zebrafish compared with KQ**I**EIK**K**FK in human). However, the differences are conservative in nature. Moreover, the two amino acids identified as important for Gap19 activity are identical in the two sequences (I130 and K134, in bold in the sequences above, Wang et al., 2013), suggesting that Gap19 probably inhibits Cx43 hemichannel activity. Because the peptide must enter the cell in order to function, we used TAT-Gap19. TAT is the transactivator of transcription motif that allows the TAT-Gap19 peptide to cross the plasma membrane (Abudara et al., 2014). We injected the TAT-Gap19 into half of the fin rays of wild-type regenerating fin at 72 hpa, leaving the other half as an internal control. Immunofluorescence using an anti-TAT antibody showed the presence of TAT-Gap19 inside the mesenchymal cells at 24 h post-injection (Fig. S2A). Following the injection of TAT-Gap19 in half of the fin rays, we found no significant decrease in regenerate length or segment length between the TAT-Gap19-injected side of the fin and the uninjected side (Fig. S2B,C). This suggests that the Cx43 hemichannel activity does not contribute to the segment length and regenerate length during fin regeneration. However, independent confirmation that Gap19 inhibits zebrafish Cx43 hemichannel activity should be performed.

DISCUSSION

The findings presented here continue to provide new insights into the molecular mechanism(s) underlying correct joint positioning in the skeleton. Previous studies demonstrated that Cx43 activity in the medial blastema is responsible for influencing joint formation in the lateral SPCs (Dardis et al., 2017). We have also shown that Cx43 influences Smp/β-catenin in the lateral SPCs, which in turn suppresses *evx1* expression and joint formation (Bhattacharya et al., 2018). Here, we demonstrate that Cx43-GJIC is responsible for promoting Smp/β-catenin signaling in the lateral SPCs, thereby inhibiting *evx1* expression and joint formation. First, we showed that inhibition of Cx43-GJIC mimics the *sof*^{b123} phenotypes of short segment length, short regenerate length and reduced cell proliferation. We next showed that inhibition of Cx43-GJIC leads to reduced *smp* expression and reduced active β-catenin. Moreover, *evx1* expression increases upon inhibition of Cx43-GJIC. We also showed that the *cx43*^{lh10} mutant (i.e. increased Cx43 protein due to

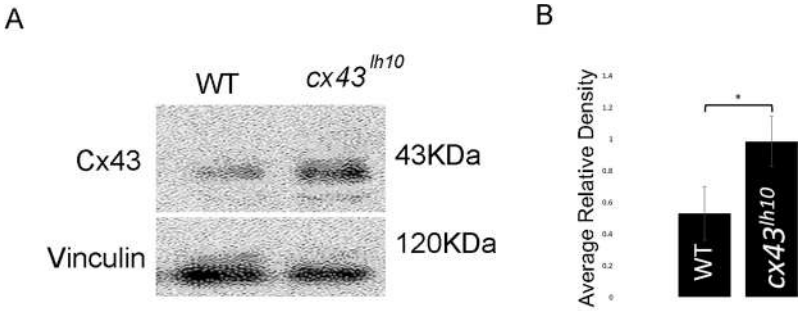

Fig. 5. The *cx43*^{lh10} allele exhibits increased Cx43 protein levels. (A) Immunoblots showing increased total Cx43 protein levels in *cx43*^{lh10} fin lysates compared with wild type (WT). (B) Bar graph showing the average relative densities of the Cx43 bands between experimental and control samples from three biological replicates. The amount of Cx43 is increased by 45% *cx43*^{lh10} lysates. Student's *t*-test, two tailed and unpaired, **P*<0.05. Ten fins per lysate; three independent replicates. Data are mean±s.d.

Development (2020) 147, dev190512. doi:10.1242/dev.190512

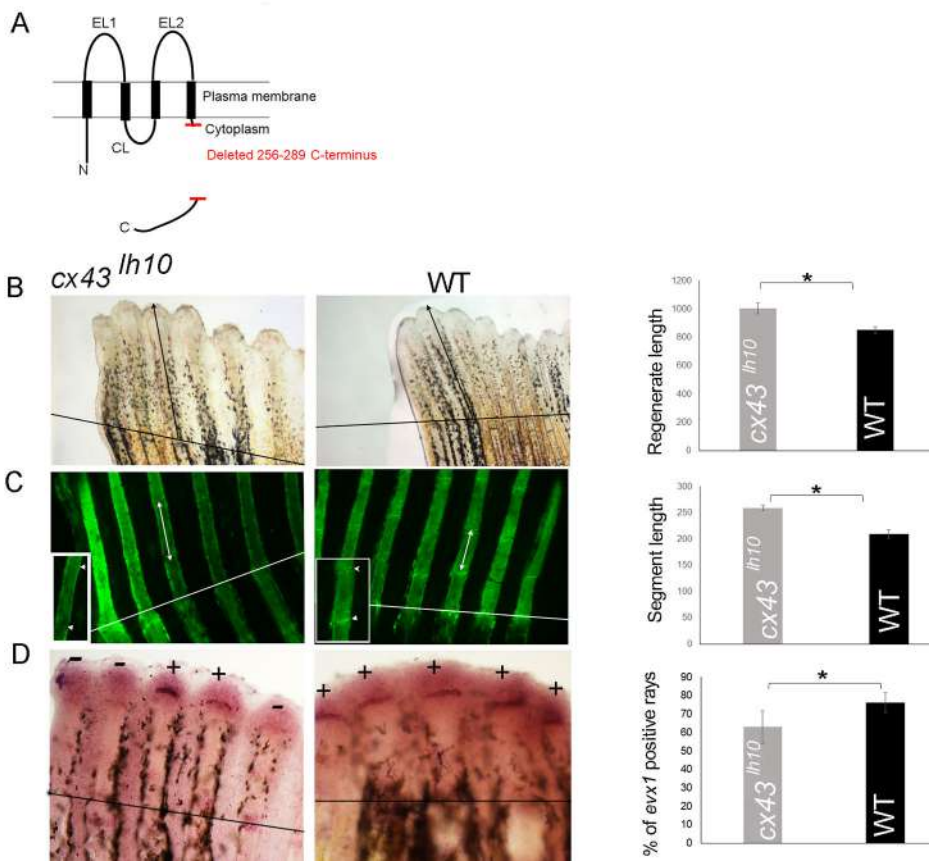

Fig. 6. The *cx43^{lh10}* allele exhibits Cx43 overexpression phenotypes. (A) Schematic of Cx43 protein showing the location of the carboxy-tail deletion. N, amino terminus; C, carboxy terminus; EL1/EL2, extracellular loop1/2; CL, cytoplasmic loop. (B) Regenerating fins in *cx43^{lh10}* mutants exhibit longer regenerate length compared with wild type (WT). All fins were amputated at the 50% level. The amputation plane is indicated (black line). Black arrows indicate the distance from the amputation plane to the distal tip of the third fin ray. Bar graph shows a significant reduction in regenerate length between *cx43^{lh10}* and wild type (Student's *t*-test, two tailed and unpaired, **P*<0.05). *n*=22; three independent replicates. (C) Regenerating fins in *cx43^{lh10}* mutants exhibit longer fin ray segments compared with wild type. Arrows and arrowheads point to the first two joints following the amputation plane (white line). The inset shows a higher magnification of the segments. Bar graph reveals a significant reduction in segment length between *cx43^{lh10}* and wild type (Student's *t*-test, two-tailed and unpaired, **P*<0.05). *n*=23; three independent replicates. (D) Regenerating fins in *cx43^{lh10}* mutants exhibit reduced *evx1* expression compared with wild type. + indicates fin rays positive for *evx1*; – indicates fin rays negative for *evx1*. Bar graph shows the percentage of *evx1*$^{+}$ fin rays is reduced in *cx43^{lh10}* compared with wild type. Student's *t*-test, two tailed and unpaired, **P*<0.05. (*n*=10; three independent replicates). Data are mean±s.e.m.

reduced Cx43 turnover) exhibits increased regenerate length and segment length compared with wild-type regenerating fins. Importantly, these phenotypes were rescued by inhibition of Cx43-GJIC, indicating that the observed gain-of-function phenotypes in *cx43^{lh10}* are probably the result of increased Cx43-GJIC.

From these findings, we propose that Cx43-GJIC in the medial blastema influences cell fate decisions in the lateral SPCs (Fig. 8). The levels of *cx43* mRNA oscillate during joint morphogenesis, which probably contributes to the level of Cx43-GJIC. Moreover, we have previously suggested that Cx43 must drop below a threshold to trigger joint formation (Dardis et al., 2017). Thus, we

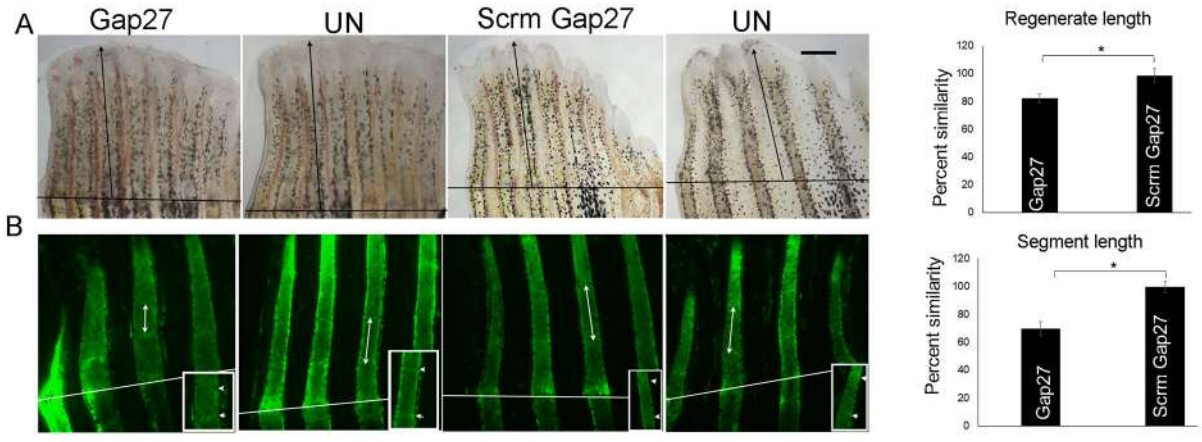

Fig. 7. Inhibition of Cx43-GJIC rescues *cx43^{lh10}* phenotypes. (A) Gap27 injection rescues regenerate length in *cx43^{lh10}* fins. Fins were amputated at the 50% level. The amputation plane is indicated (black line). Black arrows indicate the distance from the amputation plane to the distal tip of the third fin ray. Bar graph shows reduced regenerate length in *cx43^{lh10}* fins injected with Gap27 compared with *cx43^{lh10}* fins injected with Scrm-Gap27 (Student's *t*-test, two tailed and unpaired, **P*<0.05). *n*=14; three independent replicates. (B) Gap27 injection rescues segment length in *cx43^{lh10}* fins. Representative images are shown. Arrows and arrowheads point to the first two joints following the amputation plane (white line). The inset shows a higher magnification of the segments. Bar graph shows reduced segment length in *cx43^{lh10}* fins injected with Gap27 compared with *cx43^{lh10}* fins injected with Scrm-Gap27. Student's *t*-test, two-tailed and unpaired, **P*<0.05 (*n*=14, three independent replicates). Data are mean±s.e.m. Scale bar: 50 µm.

Development (2020) 147, dev190512. doi:10.1242/dev.190512

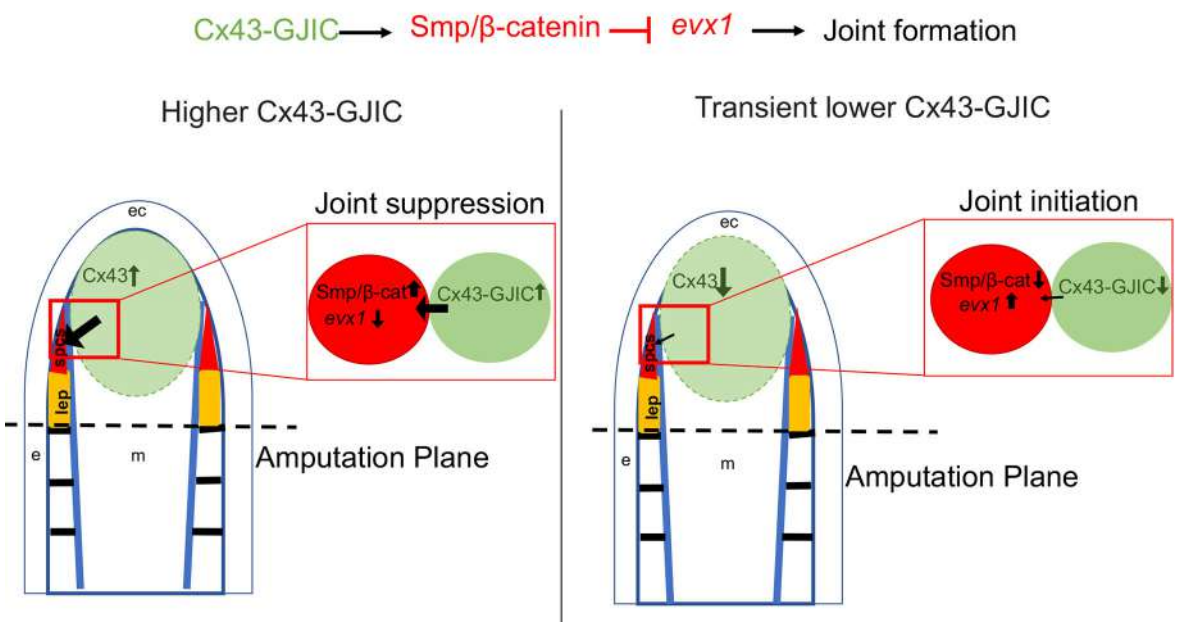

Fig. 8. Model for the role of Cx43-GJIC in influencing cell fate in SPCs. Proposed molecular pathway shown at the top. Cx43 is expressed in the medial blastema (green), and its function in the medial blastema is sufficient to regulate segment length. SPCs (red) are lateral. m, mesenchyme; e, epidermis; ec epidermal cap. Yellow (lep) indicates zone of differentiated osteoblasts. Red boxes show an expanded view of interactions between medial and lateral cells. When Cx43-GJIC is relatively high, *smp* and β-catenin increase and *evx1* decreases (left). This disfavors joint formation in SPCs. When Cx43-GJIC is reduced, *smp* and β-catenin decrease and *evx1* increases (right). This favors joint formation in SPCs.

propose that relatively higher Cx43-GJIC favors *smp*/β-catenin (inhibiting *evx1*) and favors SPC differentiation into osteoblasts. In contrast, relatively lower Cx43-GJIC inhibits *smp*/β-catenin, thereby permitting *evx1* expression and favoring SPC differentiation into joint-forming cells. The identity of the partner connexin protein in the SPCs is unknown, although Cx43 is expressed in a discrete group of SPCs (Sims et al., 2009).

The identity of the relevant small molecule signal that is transduced by GJIC is also unknown. Interestingly, gap junctions are known to propagate changes in membrane potential (i.e. V_{mem}) among coupled cells (reviewed by Levin et al., 2017; Tuszynski et al., 2017). Increasing evidence reveals that such bioelectric cues influence varied cellular behaviors, including cell differentiation and patterning (i.e. Blackiston et al., 2011; Pai et al., 2012). For example, gap junctions integrate molecular cues (such as extracellular signaling molecules) and bioelectric signals (such as changes in membrane potential or V_{mem}) as a way to regulate pattern formation (Mathews and Levin, 2016; McLaughlin and Levin, 2018). Indeed, because direct communication is restricted to coupled cells, the size and composition of the gap junction network directs specific signals to specific cells. Therefore, an attractive possibility is that Cx43-GJIC transduces changes in V_{mem} experienced by mesenchymal cells to the lateral SPCs. This in turn might activate voltage-regulated channels or voltage-dependent enzymes in SPCs that influence changes in gene expression. Evidence that such bioelectric signaling contributes to skeletal growth and regeneration comes from the alf^{dty86} mutant. Phenotypes in alf^{dty86} are caused by gain-of-function mutations in the potassium channel *kcnk5b* that lead to membrane hyperpolarization (Perathoner et al., 2014).

We also found that Smp and Sema3d, although both previously shown to act downstream of *cx43*, do not function in a common pathway. In addition, it appears that Sema3d does not depend on Cx43-GJIC. These data might suggest that an alternate activity of Cx43 promotes changes in *sema3d* expression. Although we did not find evidence that Cx43-hemichannel activity contributes to skeletal regeneration or joint formation, the scaffolding function of Cx43 could be involved. The Cx43-carboxy terminus (Cx43-CT) has been shown to function as a platform for signaling molecules such as ERK, PKCδ and β-catenin (Moorer et al., 2017). Active forms of ERK, PKCδ and β-catenin were found to be reduced in osteoblasts of the transgenic mouse lacking the entire Cx43-CT (i.e. $Gja1^{-/K258Stop}$). These mice also exhibit skeletal phenotypes consistent with a loss of Cx43 function in osteoblasts, indicating that one or more of these signaling pathways is required for mediating Cx43 function independently of Cx43-GJIC. It will be of interest to discover whether the zebrafish Cx43-CT also contributes to skeletal regeneration and if *sema3d* expression depends on this function of Cx43.

Our future studies will also address how Cx43-GJIC is regulated in the mesenchyme to control the alternating differentiation of osteoblasts (that produce bony segments) and joint-forming cells (that produce joints). We have observed that *cx43* mRNA levels are transiently reduced coincident with joint initiation (Dardis et al., 2017), although this does not preclude the possibility that Cx43 is regulated in multiple ways. Furthermore, we plan to explore whether Cx43-GJIC is responsible for transducing changes in V_{mem} and, if so, how such changes lead to changes in gene expression in SPCs.

MATERIALS AND METHODS

Fish maintenance

Zebrafish (*Danio rerio*) were maintained in a water system (Aquatic Habitats) at 27°C to 28°C in a 14:10 light:dark period (Westerfield, 2007). Water quality was monitored and dosed to maintain conductivity (400-600 ms) and pH (6.95). Research was performed in accordance with the Institutional Animal Care and Use Committee guidelines for Lehigh University (protocol 187). Food was provided three times a day. The fish were fed brine shrimp (hatched from INVE artemia cysts) once a day and flake food (Aquatox AX5) supplemented with 7.5% Micro Pellets (Hikari),

Development (2020) 147, dev190512. doi:10.1242/dev.190512

7.5% Golden Pearl (300-500 µm, Brine Shrimp Direct) and 5% Cyclop-eeze (Argent) twice a day.

Zebrafish strains

We used an equal number of C32 male and female fish, aged between 6 months and 1 year. For caudal fin amputations, fish were first anesthetized in 0.1% tricaine solution and their caudal fin rays were amputated to the 50% level. Fins were allowed to regenerate until the desired time period, depending on the requirement of the experiments. Depending on the experimental design, the regenerated fins were harvested and fixed in 4% paraformaldehyde (PFA) prepared in PBS overnight at 4°C. After fixation, fins were dehydrated in 100% methanol and stored at −20°C.

Generation of Cx43$^{\Delta 256\text{-}289}$ transgenic fish

A transgenic line was generated that deleted amino acids 256-289 in the C-terminus of Cx43 using the CRISPR/Cas9 system (i.e. this allele has been named *cx43*^{lh10}). To generate the deletion, two gRNAs were designed using the CHOPCHOP web tool (Labun et al., 2019). One gRNA was designed to target the C-terminal T256 region and the other gRNA was designed to target the C-terminal A289 region of the gene. Once designed, the gRNAs were purchased from GenScript (gRNA T256, UAGACAGUUCCUUCG-GCGUG; gRNA A289, CCAGGCUACAAACUGGCCAC; SC1838 and SC1933, respectively). Cas9 protein (12 µg, GenScript, Z03389) and each gRNA (30 pmol) were co-injected into one-cell-stage wild-type embryos. At 24 h postfertilization, 20% of embryos were genotyped using PCR and sequencing.

The remaining embryos were raised to adulthood and outcrossed to wild-type fish for the detection of germline transmission. Heterozygous embryos were then raised to adulthood and intercrossed to generate homozygous *cx43*^{lh10} mutant fish.

Peptide injections into regenerating fins

Peptides used in this study include: Gap27 (Tocris, 1476), 5Fam-Gap27, scrambled Gap27 peptide and TAT-Gap19 (YGRKKRRQRRR-KQIEIKKFK, Tocris, 6227). Fins at 3 dpa were injected with 0.5 mM peptide using the Narishige IM 300 Microinjector. Peptides (∼50 nl) were injected into each ray at the dorsal side of the regenerating fin (approximately the first five to six bony fin rays), keeping the other side uninjected as the internal control. Fins were harvested and processed at 4 dpa (24 h post-injection).

Fins injected with 5FAM-Gap27 or TAT-Gap19 were fixed in 4% PFA solution overnight and dehydrated in 100% methanol and stored at −20°C. Next, fins were embedded in 1.5% agarose/5% sucrose/PBS and equilibrated in 30% sucrose solution overnight. The fins were mounted in optimal cutting temperature medium and cryosectioned (15 µm) using a Reicherta-Jung 2800 Frigocut cryostat. Sections were collected on SuperFrost Plus slides (Fisher Scientific) and allowed to air dry overnight at room temperature protected from light. Sections were stored at −20°C. Before imaging or immunostaining, slides were brought to room temperature for 1 h and then rehydrated by three PBS washes. Slides with 5Fam-Gap27-injected fin sections were stained with DAPI, then mounted in 100% glycerol and imaged using confocal microscopy (Zeiss) at 25× using an Argon laser (488). Slides with TAT-Gap19 fin sections were processed for immunofluorescence. The slides were transferred to blocking solution [2% bovine serum albumin (BSA), 0.1% Triton X-100 in PBS] for 1 h and then incubated in anti-TAT antibody (Sigma-Aldrich, GW10817F, 1:100) overnight at 4°C. Following three PBS washes, sections were incubated with anti-chicken Alexa Fluor 488 (Invitrogen, A11039, 1:200) and DAPI for 1 h at room temperature. After three 15 min washes in blocking solution, sections were mounted with glycerol and imaged using a confocal microscope (Zeiss) at 25× with an Argon laser (488 nm).

MO-mediated gene knockdown

All MOs used in the experiments were fluorescein-tagged and purchased from Gene Tools. The MOs were reconstituted in sterile water to 1 mM. The *smp-1* MO has been described previously (Kizil et al., 2009) and validation completed in previous studies (Bhattacharya et al., 2018). The *sema3d*-MO has also been described and validated previously (Govindan et al., 2016; Ton and Iovine, 2012). The standard control MO was used as a negative control. Microinjection and electroporation procedures were carried out as described previously (Thummel and Iovine, 2017). Briefly, caudal fins were amputated at the 50% level. At 3 dpa, fish were anesthetized and MOs were injected using a Narishige IM 300 Microinjector. MO (∼50 nl) was injected into each ray at either the dorsal or ventral side of the regenerating fin tissue (the first five to six bony fin rays), keeping the other side uninjected as the internal control. Immediately after injection, both sides of the caudal fin were electroporated using a CUY21 Square Wave electroporator (Protech International). The following parameters were used during electroporation: ten 50 ms pulses of 15 V with a 1 s pause between pulses. After 1 day post-electroporation (dpe), which is equivalent to 4 dpa, the injected side of the fins were evaluated by fluorescence using a Nikon Eclipse 80i Microscope to confirm MO uptake.

Regenerate length, segment length and H3P analysis

Fins were stained with the vital dye calcein before regenerate length and segment length were measured (Du et al., 2001; Sims et al., 2009). Fish swam in 0.2% calcein (pH 7) at room temperature and were then returned to fresh water. The anesthetized fish were imaged using a Nikon Eclipse 80i Microscope equipped with a SPOT-RTKE digital camera (Diagnostic Instruments) and SPOT software (Diagnostic Instruments). Regenerate length and segment length were measured from the third fin ray from the ventralmost or dorsalmost lobe of the caudal fin (Iovine and Johnson, 2000). Regenerate length was measured from the amputation plane to the distal tip. Segment length was measured as the distance between the first two joints flanking the first complete segment.

For H3P analysis, the fins were harvested at 4 dpa (24 h post-injection/electroporation), fixed overnight in 4% PFA in PBS at 4°C and dehydrated in 100% methanol. Fins were rehydrated in progressive methanol/PBS washes, incubated in blocking solution (2% BSA and 0.1% Triton X-100 in PBS) for 1 h at room temperature, followed by incubation in anti-H3P antibody (Millipore, 06-570, 1:200) overnight at 4°C. After three PBS washes, fins were incubated with anti-rabbit Alexa 546 (Invitrogen, A11010, 1:200) for 2 h at room temperature. Fins were washed three times with PBS before being mounted on slides in glycerol. H3P^{+} cells were counted from the distalmost 250 µm of the third fin ray from the injected dorsal and uninjected ventral sides (Govindan et al., 2016). For each experiment, seven to ten fish were used per trial and at least three independent trials were performed.

Statistical analyses

The SPSS software package was used to test all data for normality. First, skewness and kurtosis values indicated that the data did not differ significantly from normality (i.e. z values were within range of ±1.96). Second, we completed Shapiro–Wilk's tests (P<0.05) (Razali and Wah, 2011). GraphPad software (www.graphpad.com) was used for Student's t-tests and for ANOVA tests. The Student's t-test (two-tailed, unpaired) was performed to test for significance between two groups (P<0.05). The one-way ANOVA was used to test for significance between three groups (P<0.001) with Tukey's and Dunnett's multiple comparison post-hoc tests (Prism version 8 software downloaded from www.graphpad.com).

In situ hybridization

Antisense digoxigenin-labeled probes were generated as described previously [Kizil et al., 2009 (smp); Ton and Iovine, 2013 (*evx1*)]. Whole-mount *in situ* hybridization was performed on harvested fins as described previously (Sims et al., 2009). To evaluate the relative level of gene expression, whole-mount *in situ* hybridization was completed on four fins in each of three independent trials.

Preparation of protein lysates and immunoblotting

Fins were amputated at 50% (ten fins per lysate, prepared in triplicate) and harvested at 3 dpa (i.e. for Cx43 in wild type versus *cx43*^{lh10}) or 4 dpa (i.e. 24 h post Gap27 or Scrm-Gap27 injection). Fin tissue was homogenized using a Bio-Gen PRO200 homogenizer at speed setting 3 for 5 s with 10 s cooling intervals in the CER buffer (cytoplasmic extraction reagent, Thermo Scientific). Homogenized samples were centrifuged at 200 ***g*** for 10 min at

4°C and supernatant protein levels normalized according to Bradford assays. Following SDS-PAGE, gels were transferred to a polyvinylidene difluoride membrane. For β-catenin and tubulin detection, blots were incubated in 2% BSA/tris-buffered saline and Tween 20 (TBST) for 1 h at room temperature followed by incubation in primary antibody (diluted in 2% BSA/TBST) overnight at 4°C. Anti-non-phosphorylated (i.e. active) β-catenin antibody (Cell Signaling, 8814, rabbit mAB used at 1:1000) was used to detect active β-catenin. Mouse monoclonal anti-tubulin antibody (Sigma-Aldrich, T9026, 1:1000) was used as a loading control. Fluorescent secondary antibodies were used for detection (anti-rabbit Alexa-488 at 1:2000 and anti-mouse Alexa 647 at 1:1000) in conjunction with Image Lab software (Bio-Rad). For Cx43 and vinculin detection, blots were incubated in 5% non-fat dry milk/TBS for 1 h at room temperature, followed by incubation in primary antibody (diluted in 5% BSA/TBS) overnight at 4°C. The Cx43 antibody (Cell Signaling Technology, 3512S) was used at a dilution of 1:2000 followed by goat anti-rabbit HRP (Invitrogen, G21234) at 1:2000. The vinculin antibody (Sigma-Aldrich, V9131) was used at a dilution of 1:5000 followed by goat anti-mouse HRP (Invitrogen, G21040) at 1:5000. Blots were incubated in enhanced chemiluminescence buffer [100 mM Tris (pH 8.8), 2.5 mM luminol, 0.4 mM p-coumaric acid and 0.02% hydrogen peroxide] before exposure to film.

ImageJ software was used to measure the band intensities. Relative pixel densities of gel bands were measured using a gel analysis tool in ImageJ software as described previously (Banerji et al., 2017). The density of each band was obtained as the area under the curve. For relative density calculation , the density of the Cx43 or β-catenin bands in the experimental samples were first normalized against the density of bands from the control samples (i.e. wild type or Scrm-Gap27). Relative pixel density was calculated as the ratio of Cx43 or β-catenin with respect to the internal control. The percent reduction was calculated by subtracting the relative pixel density from 1 and multiplying by 100. The average percent reduction with standard deviation was reported in the text. The Student's *t*-test (two-tailed, unpaired) was performed on the relative densities to test for statistical significance ($P<0.05$).

Acknowledgements
The authors thank Rebecca Bowman for the care of the zebrafish colony; members of the Iovine and Falk labs; and the Lehigh University Biological Science Department for supporting this research.

Competing interests
The authors declare no competing or financial interests.

Author contributions
Conceptualization: S.B., M.M.F., M.K.I.; Methodology: S.B., C.H.; Validation: S.B., C.H., M.K.I.; Formal analysis: S.B., C.H.; Investigation: S.B., C.H.; Writing - original draft: S.B.; Writing - review & editing: S.B., C.H., M.M.F., M.K.I.; Supervision: M.M.F., M.K.I.; Project administration: M.K.I.; Funding acquisition: M.K.I., M.M.F.

Funding
This work was supported by the National Institutes of Health (R15-HD080507 to M.K.I. and R01-GM5525 to M.M.F.). Deposited in PMC for release after 12 months.

Supplementary information
Supplementary information available online at
https://dev.biologists.org/lookup/doi/10.1242/dev.190512.supplemental

References
Abudara, V., Bechberger, J., Freitas-Andrade, M., De Bock, M., Wang, N., Bultynck, G., Naus, C. C., Leybaert, L. and Giaume, C. (2014). The connexin43 mimetic peptide Gap19 inhibits hemichannels without altering gap junctional communication in astrocytes. *Front. Cell. Neurosci.* **8**, 306. doi:10.3389/fncel.2014.00306

Banerji, R., Skibbens, R. V. and Iovine, M. K. (2017). Cohesin mediates Esco2-dependent transcriptional regulation in a zebrafish regenerating fin model of Roberts Syndrome. *Biol. Open* **6**, 1802-1813. doi:10.1242/bio.026013

Bhattacharya, S., Gargiulo, D. and Iovine, M. K. (2018). Simplet-dependent regulation of β-catenin signaling influences skeletal patterning downstream of Cx43. *Development* **145**, dev166975. doi:10.1242/dev.166975

Blackiston, D., Adams, D. S., Lemire, J. M., Lobikin, M. and Levin, M. (2011). Transmembrane potential of GlyCl-expressing instructor cells induces a neoplastic-like conversion of melanocytes via a serotonergic pathway. *Dis. Model. Mech.* **4**, 67-85. doi:10.1242/dmm.005561

Borday, V., Thaeron, C., Avaron, F., Brulfert, A., Casane, D., Laurenti, P. and Geraudie, J. (2001). evx1 transcription in bony fin rays segment boundaries leads to a reiterated pattern during zebrafish fin development and regeneration. *Dev. Dyn.* **220**, 91-98. doi:10.1002/1097-0177(2000)9999:9999<::AID-DVDY1091>3.0.CO;2-J

Dardis, G., Tryon, R., Ton, Q., Johnson, S. L. and Iovine, M. K. (2017). Cx43 suppresses evx1 expression to regulate joint initiation in the regenerating fin. *Dev. Dyn.* **246**, 691-699. doi:10.1002/dvdy.24531

Du, S. J., Frenkel, V., Kindschi, G. and Zohar, Y. (2001). Visualizing normal and defective bone development in zebrafish embryos using the fluorescent chromophore calcein. *Dev. Biol.* **238**, 239-246. doi:10.1006/dbio.2001.0390

Fong, J. T., Kells, R. M. and Falk, M. M. (2013). Two tyrosine-based sorting signals in the Cx43 C-terminus cooperate to mediate gap junction endocytosis. *Mol. Biol. Cell* **24**, 2834-2848. doi:10.1091/mbc.e13-02-0111

Goodenough, D. A., Goliger, J. A. and Paul, D. L. (1996). Connexins, connexons, and intercellular communication. *Annu. Rev. Biochem.* **65**, 475-502. doi:10.1146/annurev.bi.65.070196.002355

Govindan, J., Tun, K. M. and Iovine, M. K. (2016). Cx43-dependent skeletal phenotypes are mediated by interactions between the Hapln1a-ECM and Sema3d during fin regeneration. *PLoS ONE* **11**, e0148202. doi:10.1371/journal.pone.0148202

Hoptak-Solga, A. D., Nielsen, S., Jain, I., Thummel, R., Hyde, D. R. and Iovine, M. K. (2008). Connexin43 (GJA1) is required in the population of dividing cells during fin regeneration. *Dev. Biol.* **317**, 541-548. doi:10.1016/j.ydbio.2008.02.051

Iovine, M. K. and Johnson, S. L. (2000). Genetic analysis of isometric growth control mechanisms in the zebrafish caudal Fin. *Genetics* **155**, 1321-1329.

Iovine, M. K., Higgins, E. P., Hindes, A., Coblitz, B. and Johnson, S. L. (2005). Mutations in connexin43 (GJA1) perturb bone growth in zebrafish fins. *Dev. Biol.* **278**, 208-219. doi:10.1016/j.ydbio.2004.11.005

Jiang, J. X. and Gu, S. (2005). Gap junction- and hemichannel-independent actions of connexins. *Biochim. Biophys. Acta* **1711**, 208-214. doi:10.1016/j.bbamem.2004.10.001

Kizil, C., Otto, G. W., Geisler, R., Nüsslein-Volhard, C. and Antos, C. L. (2009). Simplet controls cell proliferation and gene transcription during zebrafish caudal fin regeneration. *Dev. Biol.* **325**, 329-340. doi:10.1016/j.ydbio.2008.09.032

Kizil, C., Kuchler, B., Yan, J.-J., Ozhan, G., Moro, E., Argenton, F., Brand, M., Weidinger, G. and Antos, C. L. (2014). Simplet/Fam53b is required for Wnt signal transduction by regulating beta-catenin nuclear localization. *Development* **141**, 3529-3539. doi:10.1242/dev.108415

Labun, K., Montague, T. G., Krause, M., Torres Cleuren, Y. N., Tjeldnes, H. and Valen, E. (2019). CHOPCHOP v3: expanding the CRISPR web toolbox beyond genome editing. *Nucleic Acids Res.* **47**, W171-W174. doi:10.1093/nar/gkz365

Levin, M., Pezzulo, G. and Finkelstein, J. M. (2017). Endogenous bioelectric signaling networks: exploiting voltage gradients for control of growth and form. *Annu. Rev. Biomed. Eng.* **19**, 353-387. doi:10.1146/annurev-bioeng-071114-040647

Mathews, J. and Levin, M. (2016). Gap junctional signaling in pattern regulation: physiological network connectivity instructs growth and form. *Dev. Neurobiol.* **77**, 643-673. doi 10.1002/dneu.22405, 643-673

McLaughlin, K. A. and Levin, M. (2018). Bioelectric signaling in regeneration: mechanisms of ionic controls of growth and form. *Dev. Biol.* **433**, 177-189. doi:10.1016/j.ydbio.2017.08.032

Moorer, M. C., Hebert, C., Tomlinson, R. E., Iyer, S. R., Chason, M. and Stains, J. P. (2017). Defective signaling, osteoblastogenesis and bone remodeling in a mouse model of connexin 43 C-terminal truncation. *J. Cell Sci.* **130**, 531-540. doi:10.1242/jcs.197285

Pai, V. P., Aw, S., Shomrat, T., Lemire, J. M. and Levin, M. (2012). Transmembrane voltage potential controls embryonic eye patterning in Xenopus laevis. *Development* **139**, 313-323. doi:10.1242/dev.073759

Perathoner, S., Daane, J. M., Henrion, U., Seebohm, G., Higdon, C. W., Johnson, S. L., Nüsslein-Volhard, C. and Harris, M. P. (2014). Bioelectric signaling regulates size in zebrafish fins. *PLoS Genet.* **10**, e1004080. doi:10.1371/journal.pgen.1004080

Razali, N. M. and Wah, Y. B. (2011). Power comparisons of Shapiro-Wilk, Kolmogorov–Smirnov, Lilliefors and Anderson-Darling tests. *J. Stat. Model. Anal.* **2**, 21-33.

Rux, D., Decker, R. S., Koyama, E. and Pacifici, M. (2019). Joints in the appendicular skeleton: developmental mechanisms and evolutionary influences. *Curr. Top. Dev. Biol.* **133**, 119-151. doi:10.1016/bs.ctdb.2018.11.002

Sáez, J. C., Retamal, M. A., Basilio, D., Bukauskas, F. F. and Bennett, M. V. L. (2005). Connexin-based gap junction hemichannels: gating mechanisms. *Biochim. Biophys. Acta* **1711**, 215-224. doi:10.1016/j.bbamem.2005.01.014

Schulte, C. J., Allen, C., England, S. J., Juárez-Morales, J. L. and Lewis, K. E. (2011). Evx1 is required for joint formation in zebrafish fin dermoskeleton. *Dev. Dyn.* **240**, 1240-1248. doi:10.1002/dvdy.22534

Sims, K., Jr, Eble, D. M. and Iovine, M. K. (2009). Connexin43 regulates joint location in zebrafish fins. *Dev. Biol.* **327**, 410-418. doi:10.1016/j.ydbio.2008.12.027

Stewart, S., Gomez, A. W., Armstrong, B. E., Henner, A. and Stankunas, K. (2014). Sequential and opposing activities of Wnt and BMP coordinate zebrafish bone regeneration. *Cell Rep.* **6**, 482-498. doi:10.1016/j.celrep.2014.01.010

Thummel, R. and Iovine, M. K. (2017). Using morpholinos to examine gene function during fin regeneration. *Methods Mol. Biol.* **1565**, 79-85. doi:10.1007/978-1-4939-6817-6_7

Ton, Q. V. and Iovine, M. K. (2012). Semaphorin3d mediates Cx43-dependent phenotypes during fin regeneration. *Dev. Biol.* **366**, 195-203. doi:10.1016/j.ydbio.2012.03.020

Ton, Q. V. and Iovine, M. K. (2013). Identification of an evx1-dependent joint-formation pathway during FIN regeneration. *PLoS ONE* **8**, e81240. doi:10.1371/journal.pone.0081240

Tu, S. and Johnson, S. L. (2011). Fate restriction in the growing and regenerating zebrafish fin. *Dev. Cell* **20**, 725-732. doi:10.1016/j.devcel.2011.04.013

Tuszynski, J., Tilli, T. M. and Levin, M. (2017). Ion channel and neurotransmitter modulators as electroceutical approaches to the control of cancer. *Curr. Pharm. Des.* **23**, 4827-4841. doi:10.2174/1381612823666170530105837

Wang, N., De Vuyst, E., Ponsaerts, R., Boengler, K., Palacios-Prado, N., Wauman, J., Lai, C. P., De Bock, M., Decrock, E., Bol, M. et al. (2013). Selective inhibition of Cx43 hemichannels by Gap19 and its impact on myocardial ischemia/reperfusion injury. *Basic Res. Cardiol.* **108**, 309. doi:10.1007/s00395-012-0309-x

Warner, A., Clements, D. K., Parikh, S., Evans, W. H. and DeHaan, R. L. (1995). Specific motifs in the external loops of connexin proteins can determine gap junction formation between chick heart myocytes. *J. Physiol.* **488**, 721-728. doi:10.1113/jphysiol.1995.sp021003

Wehner, D. and Weidinger, G. (2015). Signaling networks organizing regenerative growth of the zebrafish fin. *Trends Genet.* **31**, 336-343. doi:10.1016/j.tig.2015.03.012

Wehner, D., Cizelsky, W., Vasudevaro, M. D., Özhan, G., Haase, C., Kagermeier-Schenk, B., Röder, A., Dorsky, R. I., Moro, E., Argenton, F. et al. (2014). Wnt/beta-catenin signaling defines organizing centers that orchestrate growth and differentiation of the regenerating zebrafish caudal fin. *Cell Rep.* **6**, 467-481. doi:10.1016/j.celrep.2013.12.036

Wei, Y., Yu, L., Bowen, J., Gorovsky, M. A. and Allis, C. D. (1999). Phosphorylation of histone H3 is required for proper chromosome condensation and segregation. *Cell* **97**, 99-109. doi:10.1016/S0092-8674(00)80718-7

Westerfield, M. (2007). *The Zebrafish Book: A Guide for the Laboratory use of Zebrafish (Danio rerio)*. Eugene, Oregon: University of Oregon Press.